Stabilization of cubic structure in Mn-doped hafnia

Ling Gao, Lian Zhou, Jianqing Feng, Lifeng Bai, Zhongyuan Liu, Jean-Louis Soubeyroux, Yafeng Lu

HAL Id: hal-00714963
https://hal.science/hal-00714963

Submitted on 6 Jul 2012

Manganese Doped Hafnia

Ling Gao,[1,2] Lian Zhou,[2] Jianqing Feng,[2] Lifeng Bai,[2] Chengshan
Li,[2] Zhongyuan Liu,[3] Jean-Louis Soubeyroux,[4] and Yafeng Lu[*2]

[1]*Northeastern University, Wenhua Road, Shenyang 110819, P. R. China*
[2]*Northwest Institute for Nonferrous Metal Research,*
P.O.Box 51, Xi'an, Shaanxi 710016, P. R. China
[3]*State Key Laboratory of Metastable Materials Science and Technology,*
Yanshan University, Qinhuangdao, 066004 Hebei, P. R. China
[4]*Neel Institut, Centre National De La Recherche Scientifique,*
25, rue des Martyrs-BP 166-38042 Grenoble cedex 9, France
(Dated: February 18, 2011)

The compounds $Hf_{1-x}Mn_xO_{2-\delta}$ ($x = 0 \sim 0.5$) have been synthesized by conventional solid state reaction method in Ar. Rietveld analysis of X-ray diffraction data has shown that the Mn-doped HfO_2 undergoes a structural transformation from monoclinic to cubic phases, which is significantly dependent on the Mn content under current synthesis conditions. The stabilized cubic structure by multivalent Mn ion doping can transform to the monoclinic structure when annealed at high temperature in air. Transmission electron microscopy and electron diffraction investigations have also confirmed the existence of the high-temperature cubic structure. A mechanism of stabilizing the high-temperature cubic phase in the $Hf_{1-x}Mn_xO_{2-\delta}$ system has been analyzed based on considerations of manganese substitution effect for hafnium ions and oxygen vacancy formation.

PACS numbers: 81.05.Je, 64.60.Ci, 64.70.Kb

I. INTRODUCTION

Hafnium dioxide, as a transition metal oxide, is very important for physical and materials science communities because of potential technological applications as spintronics devices, gate dielectric in metal-oxide semiconductor devices, high-temperature fuel cell electrolytes, oxygen detectors, catalyst supports, and waveguides, although much less attention to HfO_2 has been paid during last several decades than to ZrO_2. Pure HfO_2 has three crystalline phases at ambient pressure. The monoclinic phase (m-phase) with a space group of $P2_1/c$ exists at low temperature, and transforms to a tetragonal structure (t-phase) with a space group of $P4_2/nmc$ at 1720°C, finally becomes a cubic structure (c-phase) with a space group of $Fm\bar{3}m$ at 2600°C. [1] The structural transformation temperature from stable to metastable phases for HfO_2 is even slightly higher than that for ZrO_2. Similar to that in the case of ZrO_2, many kinds of important technological applications depend on stabilization of the high-temperature phases of HfO_2 bulks or films at room temperature most probably by element doping.

A recent example is experimental and theoretical explorations of methods for realization of high dielectric constant in HfO_2. Zhao *et al.* employed density functional theory to model the undoped HfO_2 and predicted a higher permittivity in the cubic ($\kappa \sim 29$) or in the tetragonal ($\kappa \sim 70$) structures than in the monoclinic one. [2] For the Ce-doped HfO_2 a high κ was theoretically predicted for the stabilized tetragonal phase with a Ce concentration of 12.5 at. %, where the phase stability in bulks dependent on temperature, ionic radii and doping level of dopants was taken onto account. [3] Recently, $Hf_{0.5}Ti_{0.5}O_2$ was also believed to be potential a high-κ material due to enhanced dielectric responses from soft infrared-active phonon modes, [4] however, the Ti ions might serve as deep electron traps inducing localized levels in the gap and contribute to charged defects at high Ti concentrations. [5] It is interesting that reduction in charged defects associated with oxygen vacancies neutralizing the defect sites was predicted in the case of Ba incorporation into HfO_2 by Umezawa. [6] These theoretical calculations above have described one of the most promising candidates for high-κ materials applications based on the stabilized HfO_2 system. In the meantime, a lot of experimental efforts [7–11] have been made to study structural and dielectric features of pure or doped HfO_2 films on semiconducting crystalline substrates. The interface quality and the stabilization of high-temperature phases are key problems for high-performance applications.

Stabilization of the high-temperature phases in HfO_2 bulks via element doping was experimentally investigated by several groups. The single-phase region of Y-stabilized hafnia with the cubic structure is located above 8 at. % Y_2O_3 [12], where the phase boundary between the monoclinic and cubic structures lies between 6 and 8 at. % at 1500°. Research on the cubic HfO_2-R_2O_3 (R=Lu, Ho, Gd, Sm, Yb, Y and Sc) with R^{+3} ions has shown that deep vacancy trapping is responsible for the decrease in the ionic conductivity at high dopant concentrations. [13] The study of typical substitution of Ca^{+2} for Hf^{+4} has

———————
[*]Corresponding author: Tel.: + 86 29 86231079; Fax: + 86 29 86224487
E-mail address: yflu@c-nin.com (Yafeng Lu)

shown that the high-temperature electrical conductivity is dependent on the phase composition of the system. [14, 15] However, the mechanism of stabilizing of high-temperature phases in the HfO_2 has been not fully understood yet.

In regard to the aforementioned stabilization, the purpose of this study is to investigate phase transformation, microstructure, stability of HfO_2 doped by Mn ions with multivalence with a wide composition range. Our results shows importance of both element substitution and oxygen vacancy in stabilization of the high-temperature phase in the HfO_2 system.

II. EXPERIMENTAL DETAILS

The compounds $Hf_{1-x}Mn_xO_{2-\delta}$ ($x = 0 \sim 0.5$) were synthesized by a conventional solid state reaction technique using HfO_2 and MnO_2 powders (99.9% purity). The formal valence of Mn is +4 in the starting materials. After mixing the powders very carefully, the mixtures were calcined and ground again. The calcined powders were cold isostatically pressed into pellets and finally sintered at 1400°C for 12 h in argon with furnace cooling down to room temperature.

The X-ray diffraction (XRD) data were obtained with a D/max 2550 x-ray diffractometer using Cu-Kα radiation ($\lambda = 1.5406$ Å) and collected in steps of 0.020° over the 2-theta range from 10° to 80° at room temperature. The heavy griding could give rise to a phase transition of hafnia due to internal lattice strain during preparation of powder specimens for XRD measurements. In order to elucidate the effect of grinding on XRD patters, comparative XRD measurements for as-sintered bulks and ground powders were performed. The XRD profiles were refined by the Rietveld method using the fullprof software and diffraction peak profiles were refined by a pseudo-Voigt function. Thermogravimetric (TG) and differential scanning calorimetry (DSC) analyses were employed to investigate oxygen behaviors of sintered samples in the temperature range from room temperature to 1400°C. In the TG experiment, the amount of sample powders was ~ 15 mg and the heating and cooling rate was 10°C/min. Micrographs of these samples were investigated by scanning electric microscopy (SEM) and energy dispersive spectrometry (EDS) measurements were performed to quantitatively analyze the elemental composition. The microstructures were examined using a field-emission transmission electron microscope (TEM). Specimens for TEM observations were mechanically ground to a thickness of ~ 0.1 mm, further dimpled to a thickness of $\sim 10\,\mu m$ in the center, and finally ion milled to impart electron transparency.
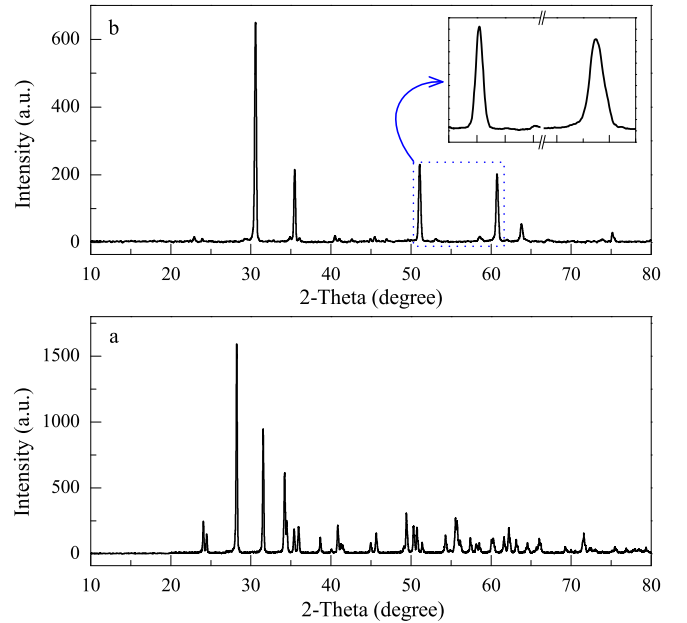

Figure 1: XRD patterns for $Hf_{0.7}Mn_{0.3}O_{2-\delta}$ sintered at 1400°C in air (a) and in Ar (b). No splitting of diffraction peaks at high angles in the inset of Fig. 1b indicates a presence of the stabilized cubic phase.

III. RESULTS AND DISCUSSION

For oxide materials, in particular for the materials in which oxygen vacancy or excess are easily formed at lattice or interstitial sites, the partial pressure of oxygen during heat treatment is a key factor to adjust structures and properties of them. Pure and doped HfO_2 by nonequivalent elements are oxygen-vacancy sensitive oxides. We first selected the sample with a nominal composition of $Hf_{0.7}Mn_{0.3}O_{2-\delta}$ to examine the influence of heat treatment atmosphere on the phase formation. XRD patterns of $Hf_{0.7}Mn_{0.3}O_{2-\delta}$ sintered at 1400°C in air and in Ar are given in Figure 1. For Mn doping content $x = 0.3$ sintered in air, only monoclinic phase is observed and no remainder manganese oxides phases are detected within the measurement limit of XRD technique, indicating that the manganese ions enter the hafnium ion sites in the monoclinic structures of HfO_2. This means that the high-temperature phases of hafnia could be not stabilized only by Mn substitution for Hf at room temperature for the sample sintered in air, even the Mn substitution content for Hf as high as $x = 0.3$. When sintered in Ar, however, the $Hf_{0.7}Mn_{0.3}O_{2-\delta}$ demonstrates a clear cubic phase as shown in Fig. 1b, where no splitting of diffraction peaks at the high angle range is found as plotted in the inset of Fig. 1b. Very sharp diffraction peaks suggest a rather high crystallinity. Here, all diffraction peaks in the Fig. 1b could be indexed according to a cubic structure with the $Fm\bar{3}m$ space group. This comparative experiment has clearly shown that besides the Mn substitution effect for Hf, the oxygen deficiency resulting
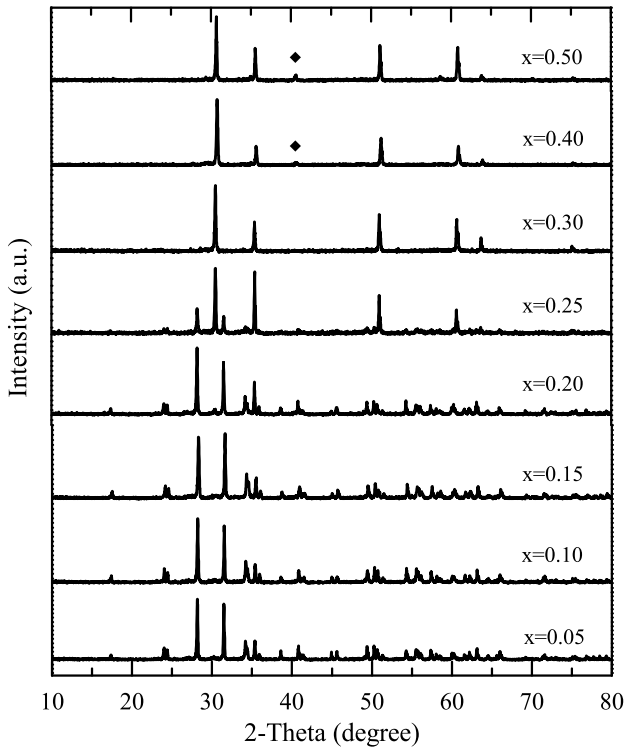
Figure 2: XRD patterns for $Hf_{1-x}Mn_xO_{2-\delta}$ with different Mn contents sintered at $1400°C$ in Ar. The transformation from the monoclinic to cubic phase occurs between $x = 0.2$ and $x = 0.3$. The residual MnO (square symbols) is detected at the high Mn concentrations.

Figure 3: XRD patterns for the as-grown sample sintered at $1400°C$ in Ar (a) and after annealing at $1000°C$ in air (b) for $Hf_{0.7}Mn_{0.3}O_{2-\delta}$. Diffraction peak of precipitated Mn_2O_3 phase after annealing is indicated by star symbol.

from sintering in Ar is an essential factor for stabilization of the high-temperature phases of hafnia. Similar results were found for the Mn-doped ZrO_2 system. [16] It should be pointed out that higher sintering temperature and lower oxygen partial pressure would not produce more obvious influences on formation and content of the high-temperature phase for the Mn-doped HfO_2 system. Therefore, sintering at $1400°C$ in Ar is a typical heat treatment condition for the subsequent experiments.

Figure 2 gives XRD profiles for the $Hf_{1-x}Mn_xO_{2-\delta}$ with different Mn contents under the same heat treatment condition. It is found that the phase constituent in the samples is divided into two apparent fields with a low Mn content ($x \leq 0.2$) and with a high Mn content ($x \geq 0.3$). For $x \leq 0.2$ the single monoclinic phase is observed, whereas for $x \geq 0.3$ the cubic phase is absolutely dominant and only for the $x = 0.4 \sim 0.5$ samples an extremely little amount of MnO remains. From the XRD patterns it is seen that the phase transformation from the monoclinic to cubic structure occurs within a very narrow composition range between $x = 0.2$ and $x = 0.3$ for the $Hf_{1-x}Mn_xO_{2-\delta}$. The $Hf_{0.75}Mn_{0.25}O_{2-\delta}$ sample just indicates a mixing of the monoclinic and cubic phases. The sudden structural change should be related to combined effects of the Mn-substitution for Hf and the oxygen vacancy. For many kinds of element doped
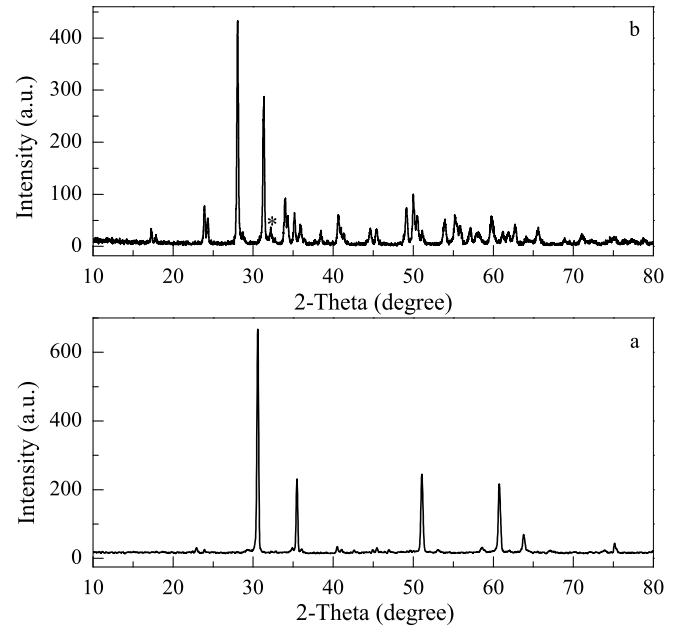
oxide compounds, this kind of abrupt structural transition dependent on doping content is rarely observed. The nearly fully separated phase components (monoclinic or cubic phases) are a good experimental platform for investigation of the magnetic Mn substitution effect in the $Hf_{1-x}Mn_xO_{2-\delta}$. All the diffraction peaks for the monoclinic and cubic phases are indexed with the $P2_1/c$ and $Fm\overline{3}m$ space group respectively. Lattice parameters and structural variation details will be discussed later.

In order to study the structural stability of high-temperature cubic phase in the $Hf_{1-x}Mn_xO_{2-\delta}$ we annealed the sintered sample with $x = 0.3$ at $1000°C$ for 8 hours in air. Their XRD patterns are indicated in Fig. 3. It is found that after annealing in air the as-sintered sample becomes monoclinic with a little amount of precipitated Mn_2O_3 phase. The SEM image of the annealed sample (not given here) shows formation of some microcracks because of relatively large internal stress originating from the structural transformation from cubic to monoclinic phases. This implies that the transition from the high-temperature to low-temperature phase is directly associated with the disappearance of oxygen vacancy during annealing in air for the Mn-doped HfO_2, although the change of oxygen vacancies could be not determined quantitatively in our case. If we carefully analyze the position of diffraction peaks after annealing and further compare the difference in the XRD peak position between the annealed samples and the $0.05 \leq x \leq 0.2$ samples, one can found that there still exists a dependence of XRD diffraction peak positions on the Mn content, which will be discussed below.
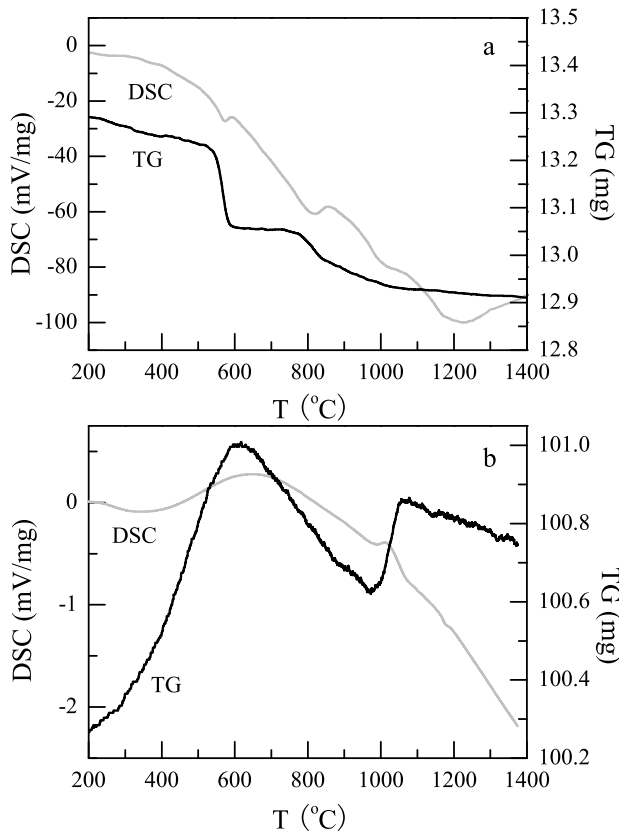
Figure 4: TG and DSC curves for $Hf_{0.7}Mn_{0.3}O_{2-\delta}$ green powder in Ar (a) and for as-grown pellet in air (b).

Figure 5: Lattice parameters and cell volume dependent on the Mn content x in $Hf_{1-x}Mn_xO_{2-\delta}$. The cell volume of transformed monoclinic phase derived from Fig. 3b is 138.07 $Å^3$. The lattice constant and cell volume of the pure cubic HfO_2 are 5.12 Å and 133.82 $Å^3$.

Further experimental investigation results of oxygen behavior on structural transformation of the $Hf_{1-x}Mn_xO_{2-\delta}$ with the help of thermal analysis technique are shown in Fig. 4. The TG curve of the $Hf_{0.7}Mn_{0.3}O_2$ green powder with a heating rate of $10°C/min$ in Ar shows a typical multi-step weight loss process. At close to 600 °C a sharp weight loss occurs. With increasing temperature the second weight loss comes out at about 800 °C and even up to 1400 °C a very slow weight loss is still seen in the TG curve. Correspondingly, there are two obvious endothermic peaks below 1000 °C and one exothermic peak above 1000 °C in the DSC curve. However, the as-grown $Hf_{0.7}Mn_{0.3}O_2$ sample with a cubic structure demonstrates a whole weight increase superposed by two distinct peaks at 600 °C and 1050 °C during heating in air as shown in Fig. 4b. In the relevant DSC curve a flat exothermic peak at low temperature and a sharp exothermic peak at high temperature are observed.

It is believed that figure 4a reflects the formation process of cubic hafnia phase with addition of Mn ions with variable valences in argon. Here we selected MnO_2 as starting material due to its good chemical stability at ambient conditions. As heated in Ar MnO_2 easily decomposes to Mn_2O_3 with a formal valence of Mn^{+3} accompanied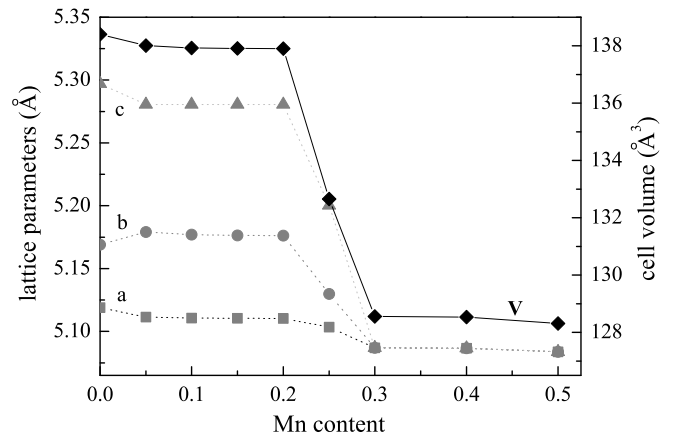 with an oxygen loss [17]. Therefore, the weight loss and the endothermic peak at close to 600 °C correspond to the valence change from Mn^{+4} to Mn^{+3}, although the measured temperature range of MnO_2 decomposition in air varied from 697 K to 943 K as reported in Refs. [17–19]. The further weight loss at about 800 °C may be related to the formation of a mixed valence of Mn^{+3} and Mn^{+2}. This temperature range is slightly lower than the values experimentally measured for Mn_2O_3 decomposition in air and oxygen, [18, 20, 21] because the decomposition temperature would lower with decreasing oxygen partial pressure as expected by the Mn-O phase diagram. [22] With incorporation of Mn^{+2} ions into Hf^{+4} sites the cubic phase in $Hf_{1-x}Mn_xO_{2-\delta}$ could be finally stabilized, although there exists a little amount of residual Mn^{+2} for the samples with high Mn concentrations as indicted in Fig. 2b. For the stabilized cubic $Hf_{0.7}Mn_{0.3}O_{2-\delta}$, we suggest that the weight increase below 600 °C in air originates from a decrease of oxygen vacancies due to the partial valence change from Mn^{+2} to Mn^{+3}. At about 600 °C the concentration of Mn^{+3} ions reaches a maximum and then Mn_2O_3 begins to precipitate due to a limited solution of Mn^{+3} in the cubic phase, but the total sample weight still is larger than that before annealing due to the increased oxygen concentration. When annealing temperature rises to 1000 °C, the transformation from cubic to monoclinic structure occurs. Meanwhile the formation of microcracks because of lattice cell volume expansion accelerates diffusion of oxygen atoms and an oxygen concentration increase is expected. The TG and DSC data above may demonstrate that the combined effect of manganese substitution and oxygen vacancy determines stabilization of the cubic phase in $Hf_{1-x}Mn_xO_{2-\delta}$.

The lattice parameters for the monoclinic and cubic phases of $Hf_{1-x}Mn_xO_{2-\delta}$ were determined using the Rietveld method based on the measured data above. During refinement a pseudo-Voigt function was chosen to
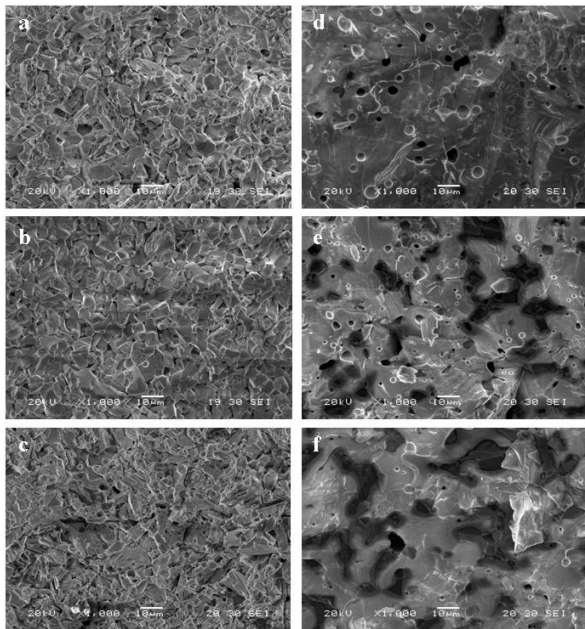
Figure 6: SEM images for $Hf_{1-x}Mn_xO_{2-\delta}$ with different Mn content (a) $x = 0.05$; (b) $x = 0.10$; (c) $x = 0.20$; (d) $x = 0.30$; (e) $x = 0.40$; (f) $x = 0.50$.

Figure 7: high-resolution transmission electron microcopy (HRTEM) image and selected area electron diffraction (SAED) pattern of as-grown $Hf_{0.7}Mn_{0.3}O_{2-\delta}$.

produce the line profile of the diffraction peaks. The adopted space groups are $P2_1/c$ and $Fm\overline{3}m$ for the monoclinic and cubic phases respectively. The derived lattice parameters dependent on the Mn content are plotted in Fig. 5. Compared to the lattice parameters of the pure HfO_2 bulk with a monoclinic structure, the b-axis slightly increases for the doped HfO_2 samples of $0.05 \leq x \leq 0.2$, whereas the a- and c-axis to some extent decreases, generally resulting in a little reduction of the crystal cell volume with increasing the Mn content. For the cubic Mn-doped HfO_2, a weaker reduction of the lattice constant and cell volume is detected. These values are much smaller than that for the pure cubic HfO_2, which was obtained by extrapolation based on theoretical expression of dependence of the lattice parameter on temperature. [24]

Figure 6 gives SEM images of fracture surfaces of the $Hf_{1-x}Mn_xO_{2-\delta}$ samples prepared at 1400 °C in Ar. We found two kinds of different morphology of grains for low Mn content ($x \leq 0.2$) and high Mn content ($x \geq 0.3$) samples. For the samples with $x \leq 0.2$ the monoclinic grains are small and dense. The cubic grains are relatively large for the $x \geq 0.3$ samples. This difference in the morphology suggests different growth mechanism of monoclinic and cubic grains in the $Hf_{1-x}Mn_xO_{2-\delta}$. Some round pores as shown in Figs. 6(d)-6(f) are due to residual air in the pellets during cold isostatical pressing. We believe that occurrence of wandering dark areas in Figs. 6(d)-6(f) may originate from partial melting of Mn_2O_3 during sintering. In fact, the EDS analysis implied the presence of these Mn-rich dark areas at high dopant concentrations.
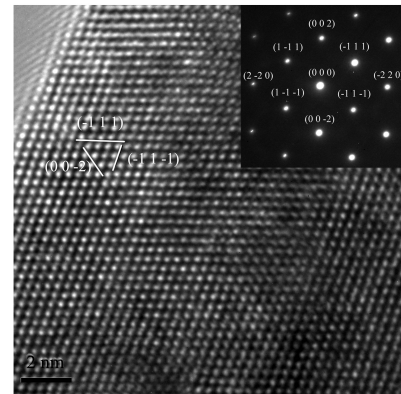
Transmission electron microscopy image provides further insight into the structure of Mn-doped HfO_2. Figure 7 shows HRTEM image and SAED pattern of the $Hf_{0.7}Mn_{0.3}O_{2-\delta}$ sample. The crystallinity within the individual grains of $Hf_{0.7}Mn_{0.3}O_{2-\delta}$ is excellent, as seen in the HRTEM image. The SAED pattern with the characteristics of the cubic structure as shown in the inset of Fig. 7 also supports the XRD analyses above.

Now we turn to discuss a possible mechanism of structural transformation from monoclinic to cubic phases in the Mn-doped HfO_2 system. The experimental results have shown that the cubic phase in the Mn-doped HfO_2 system can be stabilized by the combined effects of Mn-substitution for Hf and reduced atmosphere during sintering in Ar. The valence change of Mn ions here plays am important role in the stabilization. A few experimental studies have demonstrated a possibility of stabilization of HfO_2 high-temperature phases. M. García-Hipólito *et al.* found that 5 atomic percent of Mn in relation to the Hf content in the Mn-doped HfO_2 coatings deposited by spray pyrolysis method cannot stabilize the high-temperature phases. [25] In PLD films of Co-doped HfO_2 on (001) yttrium-stabilized zirconia (YSZ) the high-temperature phases were not obtained. [26] For atomic layer deposited $Hf_xZr_{1-x}O_2$ films a tetragonal phase cannot be observed until the ZrO_2 content is larger than 50%. [27] On p-type (100) Si/SiO_2 the Y-doped HfO_2 thin films were grown using liquid injection metal organic chemical vapor deposition, where the cubic structure of HfO_2 is stabilized for 6.5 at.%. [28] But on GaAs (001) the cubic HfO_2 phase is obtained with 19 at.% Y_2O_3 using molecular beam epitaxy. [29] For Er-doped HfO_2 (Er$\sim$ 15%) films the stabilization of the cubic structure is realized by atomic layer deposition on Si(100). [30] We believe that for doped HfO_2 films on single crystalline substrates the stabilization of high-temperature phases may be a commonly contributed result of element doping, possible oxygen vacancy, lattice mismatch strain, even surface effect. For element doped HfO_2 bulks, experimental work is lacking for understanding of the stabilization mechanism of high-temperature structures.

A basic mechanism of stabilization of high-temperature phases in element doped ZrO_2 system is already proposed based on many experimental and theoretical research results. In the case of cation substitution with the same valence for Zr^{+4}, the introduction of cations with a larger ionic radius than that of Zr^{+4} leads to an enlargement of the ZrO_2 crystalline cells and then increases stability of the high-temperature phases, whereas for cation substitutions for Zr^{+4} with lower valence elements the formation of oxygen vacancies is an essential factor for stabilization of the high-temperature phases. On the other hand, the grain size and the surface configuration in the materials are two extrinsic factors influencing stabilization of the high-temperature phases. Due to the similarity of Hf^{+4} to Zr^{+4} in chemical properties, we can analyze the process of phase transformation in the $Hf_{1-x}Mn_xO_{2-\delta}$ system with the help of stabilization mechanism in the element doped ZrO_2 system. The ionic radius of Hf^{+4} is 0.83 Å, while those of Mn^{+4} and Mn^{+2} are 0.67 Å and 0.96 Å. [23] For the equivalent Mn^{+4} cations as in the starting material of MnO_2, a much smaller ionic radius than Hf^{+4} may inactivate the effect of enlargement of crystalline cells for the stabilization. With increasing heat treatment temperature in argon the transition of the charge state of manganese from Mn^{+4} to Mn^{+2} makes it possible for stabilization effects from both enlargement of crystalline cells and introduction of oxygen vacancy defects in the HfO_2. If the nominal oxygen vacancy concentration of δ reaches 0.3, the cubic phase is finally stabilized in the HfO_2. In fact, the crystalline cell volume of the Mn-doped cubic HfO_2 ($V = 128.46$ Å^3) is much smaller than the pure cubic ZrO_2 ($V = 134.85$ Å^3) and still smaller than the theoretically calculated value of the pure cubic HfO_2 ($V = 133.82$ Å^3). [24] This suggests that the effect of oxygen vacancy defects on stabilization of the cubic structure is very important, since the cell volume of the cubic structure is in principle proportional to the concentration of oxygen vacancies in ZrO_2 or HfO_2. For doping in ZrO_2 by bivalent cations, such as Mg^{+2}, Ca^{+2}, and Sr^{+2}, however, a fully stabilized cubic structure has been not experimentally obtained.

When the stabilized cubic phase undergoes annealing in air, such as for $Hf_{0.7}Mn_{0.3}O_{2-\delta}$ as shown in Fig. 3b, the derived cell volume of transformed monoclinic phase is 138.07 Å^3, which is slightly larger than that of the pure monoclinic phase. Therefore, we believe that the combined influence of substitution of manganese for hafnium and oxygen vacancy defects resulting from the charge state transition of manganese during heat treatment in argon is responsible for the structural transformation between monoclinic and cubic phases in HfO_2. For completely understanding of the structural transformation mechanism at an atomic scale, it is necessary to experimentally investigate interacting lattice distortions due to the substitution effect, the crystallography of cubic-to-monoclinic transformations, and formation of oxygen vacancy defects in the future.

IV. CONCLUSION

In summary, we have successfully synthesized the $Hf_{1-x}Mn_xO_{2-\delta}$ ($x = 0 \sim 0.5$) bulks by conventional solid state reaction method. It has been found that with increasing the Mn content the $Hf_{1-x}Mn_xO_{2-\delta}$ system transforms from the monoclinic to cubic structure, where the charge state change of Mn accompanies the phase transformation due to the requirement of ionic size and oxygen vacancies for stabilization of high-temperature phases. The phase transformation occurs within a very narrow composition range between $x = 0.2$ and $x = 0.3$ for the $Hf_{1-x}Mn_xO_{2-\delta}$. We believe that the effects of manganese ionic size and oxygen vacancy defects all related to variable valences of Mn are important for stabilization of high-temperature phases in the Mn-doped HfO_2.

[1] J. Wang, H. P. Li and R. Stevens, J. Mater. Sci. **27**, 5397 (1992).

[2] X. Zhao and D. Vanderbilt, Phys. Rev. B **65**, 233106 (2002).

[3] D. Fischer and A. Kersch, Appl. Phys. Lett. **82**, 012908 (2008).

[4] G. Dutta, Appl. Phys. Lett. **94**, 012907 (2009).

[5] D. Ramo, A. Shluger, and G. Bersuker, Phys. Rev. B **79**, 035306 (2009).

[6] N. Umezawa, Appl. Phys. Lett. **94**, 022903 (2009).

[7] X. F. Wang, Quan Li, and M. S. Moreno, Appl. Phys. Lett. **104**, 093529 (2008).

[8] P. R. Chalker, M. Werner, S. Romani, R. J. Potter, K. Black, H. C. Aspinall, A. C. Jones, C. Z. Zhao, S. Taylor, and P. N. Heys, Appl. Phys. Lett. **93**, 182911 (2008).

[9] C. Y. Kim, S. W. Cho, M.-H. Cho, K. B. Chung, C.-H. An, H. Kim, H. J. Lee, and D.-H. Ko, Appl. Phys. Lett. **93**, 192902 (2008).

[10] V. V. Afanas′ev, M. Badylevich, A. Stesmans, G. Brammertz, A. Dealbie, S. Sionke, A. O′Mahony, I. M. Povey, M. E. Pemble, E. O′Connor, P. K. Hurley, and S. B. Newcomb, Appl. Phys. Lett. **93**, 212104 (2008).

[11] A. A. Sokolov, E. O. Filatova, V. V. Afanas′ev, V. Eu Taracheva, M. M. Brzhezinskaya, and A. A. Ovchinnikov, J. Phys. D: Appl. Phys. **42**, 035308 (2009).

[12] Jon D. Schieltz, John W. Patterson, and D. R. Wilder,

Electronchemical Science **118**, 1257 (1971).

[13] Mladen F. Trubeljia and Vladimir S. Stubican, J. Am. Ceram. Soc. **74**, 2489 (1991).

[14] A. W. Smith, F. W. Meszaros, and C. D. Amata, J. Am. Ceram. Soc. **49**, 240 (1966).

[15] H. A. Johansen and J. G. Cleary, J. Electrochem. Soc. **111**, 100 (1964).

[16] Yafeng Lu *et al.*(unpublished) (2011).

[17] H. F. McMurdie and E. Golovato, J. Res. Natl. Bur. Stand. **41**, 589 (1948).

[18] H. E. Kissinger, H. F. McMurdie, and B. S. Simpson, J. Am. Ceram. Soc. **39**, 168 (1956).

[19] M. P. Dubois and M .G. Urbain, Cryst. Rev. **199**, 1416 (1934).

[20] W. C. Hahn and A. Muan, Am. J. Sci. **258**, 66 (1960).

[21] R. J. Meyer and K. Rotgers, Z. Anorg. Chem. **57**, 104 (1908).

[22] A. Nicholas Grundy, Bengt Hallstedt and Ludwig J. Gauckler, Journal of Phase Equilibria **24**, 21 (2003).

[23] Golden Book of Phase Transitions Wroclae **1**, 1-123 (2002).

[24] lattice parameters of pure HfO2 from Lit.

[25] M. García-Hipólito, O. Alvarez-Fregoso, J. Guzmán, E. Martínez, and C. Falcony, phys. stat. sol. (a) **201**, R127 (2004).

[26] S. Dhar, M. S. Ramachandr, S. R. Shinde, T. Venkates, S. J. Welz, R. Erni, and N. D. Browning, Appl. Phys. Lett. **87**, 241504 (2005).

[27] D. H. Triyoso, R. I. Hegde, J. K. Schaeffer, D. Roan, P. J. Tobin, S. B. Samavedam, B. E. White, Jr, R. Gregory, and X.-D. Wang, Appl. Phys. Lett. **88**, 222901 (2006).

[28] E. Rauwel, C. Dubourdieua, B. Hollánder, N. Rochat, F. Ducroquet, M. D. Rossell, G. Van Tendeloo, and B. Pelissier, Appl. Phys. Lett. **89**, 012902 (2006).

[29] Z. K. Yang, W. C. Lee, Y. J. Lee, P. Chang, M. L. Huang, M. Hong, Hsi, C.-H. Hsu, and J. Kwo, Appl. Phys. Lett. **90**, 152908 (2007).

[30] C. Wiemer, L. Lamagna, S. Baldovino, M. Perego, S. Schamm-Chardon, P. E. Coulon, O. Salicio, G. Congedo, S. Spiga, and M. Fanciulli, Appl. Phys. Lett. **96**, 182901 (2010).